Structure, optical absorption, and luminescence energy calculations of Ce^{3+} defects in $LiBaF_3$

M. Marsman, J. Andriessen, and C. W. E van Eijk
Radiation Technology Group, Interfaculty Reactor Institute, Delft University of Technology, Mekelweg 15, 2629 JB Delft, The Netherlands
(Received 18 November 1999)

We address two remarkable features in the optical behavior of Ce^{3+} defects in $LiBaF_3$: the fourfold splitting of the Ce^{3+} $5d$ manifold in a cubic system, and the unusually large Stokes shift, of around 1 eV (≈ 9000 cm^{-1}), between the energy of the lowest Ce^{3+} $4f \rightarrow 5d$ absorption line and its $5d \rightarrow 4f$ luminescence energy. To this end we investigated the electronic properties and the structure of several possible luminescence center configurations in $LiBaF_3$:Ce^{3+}, each consisting of a Ce^{3+} substitution at a Ba or Li site, plus an appropriate charge-compensating defect. Using a plane-wave pseudopotential density-functional-based method to optimize the geometry of a supercell consisting of $3\times3\times3$ $LiBaF_3$ unit cells, containing a single luminescence center, the equilibrium structures of these defect complexes were determined. We performed *ab initio* cluster calculations at the Hartree-Fock level to determine the optical-absorption energies of the Ce^{3+} $4f \rightarrow 5d$ transitions in these different geometries. Comparison of these energies with the results of optical-absorption measurements on $LiBaF_3$:Ce^{3+} shows that the most likely luminescence center configuration consists of Ce^{3+} at a Ba site, charge compensated by the substitution of one of its nearest-neighboring Ba ions by a Li^+ ion. For this configuration we have repeated the cluster and supercell calculations with Ce^{3+} in the $[Xe]5d^1$ excited-state electronic configuration to determine the Ce^{3+} $5d \rightarrow 4f$ luminescence energy and to study effects that can explain the large Stokes shift in this material. These calculations predict an extensive lattice relaxation, induced by the excitation of the Ce^{3+} ion, and yield a Stokes shift of 0.61 eV (compared to 1 eV found from experiment). The origin of this large Stokes shift is identified as a strong coupling of the crystal-field splitting of the Ce^{3+} $5d$ manifold to the displacement of four of its F nearest neighbors.

I. INTRODUCTION

The increasing interest shown in recent years, in $LiBaF_3$ compounds doped with optically active ions such as Cu^+, Co^{2+}, Ni^{2+}, Pb^{2+}, or Ce^{3+}, has been mainly due to their potential applicability as lasing material.[1–5] In our group, Combes *et al.*[6] studied the optical and scintillation properties of $LiBaF_3$:Ce^{3+}, in light of its possible use as a scintillation detector for thermal neutrons.

The x-ray-induced emission spectra of pure $LiBaF_3$ show a cross luminescence (CL) contribution, with two peaks, at 190 and 225 nm, and a broad band attributed to self-trapped exciton (STE) luminescence, centered around 290 nm. When doped with Ce^{3+}, $LiBaF_3$ shows in addition to the CL and STE emission, Ce^{3+} luminescence between 300 and 400 nm. Optical-absorption measurements on $LiBaF_3$:Ce^{3+} show four bands, at 204, 218, 240, and 250 nm, attributed to $4f \rightarrow 5d$ transitions in Ce^{3+}.

Above-mentioned experimental results reveal two remarkable aspects of Ce^{3+} in $LiBaF_3$: (i) The Ce^{3+} $5d$ manifold is splitted fourfold—essentially a perturbed cubic splitting—which is noteworthy since $LiBaF_3$ is a cubic system; (ii) $LiBaF_3$:Ce^{3+} shows a Stokes shift, of around 9000 cm^{-1}, between the maximum of the Ce^{3+} emission band at 320 nm, and the absorption band at 250 nm, which is unusually large compared to, for instance, BaF_2: Ce^{3+}, where it is 2000 cm^{-1}.

The explanation of these properties of Ce^{3+} in $LiBaF_3$ constitutes quite a challenging problem for computational physicists, which has prompted a study of the geometry and electronic structure of the luminescence center in $LiBaF_3$:Ce^{3+}, by means of *ab initio* methods.

Crystalline $LiBaF_3$ has the inverse perovskite structure, with space group $Pm\bar{3}m$, and one formula unit in the unit cell ($a_0 = 3.988$ Å).[7] When Ce^{3+} is incorporated in the $LiBaF_3$ lattice, on a regular lattice site, it must be accompanied by a charge-compensating defect. We have considered as possible sites for Ce^{3+} in $LiBaF_3$, the Li site and the Ba site, which leave, respectively, excess charges of $2+$ and $1+$ to be compensated. In pure $LiBaF_3$ both sites have O_h point-group symmetry. However, the perturbed cubic splitting of the Ce^{3+} $5d$ manifold observed in experiment clearly points at a lowering of symmetry at the Ce site, most probably caused by the charge-compensating defect. The extend to which the cubic splitting is perturbed indicates that the charge compensating defect is likely to be located within the next-next-nearest-neighbor distance of the Ce^{3+} ion. In the following we will indicate the complex of a Ce^{3+} ion on a regular lattice site with an associated charge compensation by the term *luminescence center*.

Recently Andriessen *et al.*[8] used the Hartree-Fock linear combination of atomic orbitals (HF-LCAO) method with Gaussian-type orbitals, on clusters of ions consisting of the Ce ion, surrounded by one or more shells of its nearest neighbors plus the charge-compensating defect, to calculate the splitting of the Ce^{3+} $5d$ manifold in a number of possible luminescence center configurations. These were compared to the position of the Ce^{3+} bands found in optical-absorption measurements.

(i) *Ce^{3+} on a Ba site, plus an O^{2-} ion at a nearest F site.* The splitting of the $5d$ manifold is more than two times too

large, and the ordering of the levels is wrong.

(ii) *Ce^{3+} on a Ba site, plus an interstitial F^- ion in the nearest neighbor region.* The splitting of the $5d$ manifold is too large.

(iii) *Ce^{3+} on a Ba site, plus a vacancy at a nearest Li site.* The extent of the splitting of the $5d$ manifold is reasonable. However, the lowest Ce-$5d$ cubic crystal-field state in this geometry, the twofold degenerate e level, is not split up, neither by the noncubic terms in the crystal field—Ce sits at a site of C_{3v} symmetry—nor by the spin-orbit interaction. This is in disagreement with experiment. Extensive relaxation of the lattice around the Ce site, however, could affect the Ce-$5d$ cubic crystal-field states to such an extent that the ordering of the e and t_2 levels is reversed. The t_2 level will be split up threefold by the crystal field and the spin-orbit interaction, which could conceivably lead to agreement with experiment. This possibility was not explored.

(iv) *Ce^{3+} on a Ba site, plus a Li^+ at a nearest Ba site.* The splitting of the $5d$ manifold is reasonable. In this configuration of the luminescence center—twelve coordination of Ce^{3+}—the predicted splitting is very sensitive to displacements of the F^- ligands. Therefore, attempts were made to optimize the geometry of the cluster, by calculating the lattice relaxation around the Ce ion, using a pair-potential model. The description of the ion-ion interaction in this model is semiempirical, and the interaction parameters were not fitted to measurements on $LiBaF_3$ itself, which casts a large doubt on the obtained results.

(v) *A Ba vacancy compensating for two Ce^{3+} substitutions at Ba sites.* The results are quantitatively comparable to case (iv), however the extent of the splitting of the $5d$ manifold is somewhat larger, and exaggerated in comparison with experiment. Aside from this, it is likely that in this geometry, the Ce^{3+} $5d$ manifold is located in the conduction band.

(vi) *Ce^{3+} on a Li site, plus a vacancy at a nearest Ba site.* As in case (iii), the Ce site again has C_{3v} symmetry, however in this geometry the lowest Ce-$5d$ cubic crystal field state is the t_2 level, whose degeneracy is lifted by the crystal field and the spin-orbit interaction. The resulting splitting of the $5d$ manifold is fourfold, which is in agreement with experiment. However, the extent of the splitting is too large. For this luminescence center configuration a substantial relaxation of the lattice was expected, and an attempt was made to optimize the geometry of the cluster using the HF-LCAO method. Unfortunately, past experience has shown that the cluster description of the Ce defect, employed in the HF-LCAO method, is not adequate to determine the geometry of the luminescence center, because the perturbation of the lattice, induced by the dopant Ce ion and the charge-compensating defect, is not limited to the shell of nearest or next-nearest neighbors.

The above-mentioned study led Andriessen *et al.* to conclude that the configuration of the luminescence center in $LiBaF_3:Ce^{3+}$ most likely consists of Ce^{3+} at a Ba site, charge compensated by a Li^+ ion at a nearest Ba site. This conclusion, however, is not unequivocal since the reliability of both methods, employed to include the influence of lattice relaxation on the position of the Ce^{3+} energy levels, was considered to be unsatisfactory. A reliable *ab initio* treatment of lattice relaxation is needed for the unambiguous identification of the luminescence center in $LiBaF_3:Ce^{3+}$, and to reach an overall better quantitative agreement between the energy of the Ce^{3+} $4f \rightarrow 5d$ absorption lines predicted by calculations and the lines found in experiment.

Furthermore, the large Stokes shift of Ce^{3+} in $LiBaF_3$ indicates that a Ce^{3+} $4f \rightarrow 5d$ excitation is followed by a strong lattice relaxation. Attempts to use the HF-LCAO method to determine the displacements of the F^- ligands, induced by an excitation of the Ce ion, and subsequently calculate the energy of the Ce^{3+} $5d \rightarrow 4f$ emission line, have so far always underestimated the Stokes shift in $LiBaF_3:Ce^{3+}$ by at least a factor of 5.

In this paper we calculate the lattice relaxation and the energy of the Ce^{3+} $4f \rightarrow 5d$ absorption lines for Ce^{3+} on a Ba site plus a vacancy at a nearest Li site, Ce^{3+} on a Li site plus a vacancy at a nearest Ba site, and Ce^{3+} at a Ba site plus a Li^+ at a nearest Ba site. For the latter luminescence center configuration we perform separate calculations on Ce^{3+} in its $[Xe]4f^1$ ground-state configuration and Ce^{3+} in the $[Xe]5d^1$ excited-state configuration, to determine the origin of the large Stokes shift in $LiBaF_3:Ce^{3+}$.

To calculate the lattice relaxation we have employed a density-functional-based plane-wave pseudopotential method, to optimize the geometry of large supercells of $LiBaF_3$, containing a single luminescence center. While very well suited to structural optimization, these density-functional-based methods in general do not offer the best approach to the calculation of the Ce^{3+} $4f$ and $5d$ energy levels. To study the electronic structure of the luminescence center, i.e., to calculate the energy levels of Ce^{3+} in the host crystal, we have followed the same approach as Andriessen *et al.* and employ the HF-LCAO method. In total, our approach to the study of Ce^{3+} in $LiBaF_3$, therefore, consists of the combination of two complementary methods and their respective ways of modeling the Ce defect in the crystalline host. An added advantage of using two methods, each based on a different one-electron approximation to the many-electron Schrödinger equation, is found in the fact that some properties of $LiBaF_3:Ce^{3+}$, such as, for instance, the splitting of the Ce^{3+} $5d$ manifold, can be calculated with both methods. Comparison of the respective results then gives some insight into the systematic errors of both methods.

The remainder of this paper is organized as follows. Sections II, III, and V contain specifics concerning the methods we used to calculate, respectively, the spectroscopic properties of the Ce^{3+} ion and the lattice relaxation. Section IV presents the approach we used to calculate the Stokes shift. In Sec. VI results of the calculations on the three luminescence centers are presented. Conclusions and discussion can be found in Secs. VII and VIII.

II. ENERGY LEVELS

To determine the electronic structure and investigate the spectroscopic properties of the luminescence center in $LiBaF_3:Ce^{3+}$, we have performed *ab initio* quantum-chemical calculations, at the Hartree-Fock level, using the Gaussian™ G94 program.[9]

To model the luminescence center, we take a cluster of atoms out of the crystal, containing the Ce ion, one or more shells of its neighboring atoms, and the accompanying charge-compensating defect. In our calculations this cluster

TABLE I. Results of the MCDF and G94 calculations on the $[Xe]4f^1$ and $[Xe]4d^1$ configurations of free Ce^{3+} (all energies in eV).

State	MCDF		G94 (no j splitting) identification with $j=l+\frac{1}{2}$	
	Total energy	Orbital energy	Total energy	Orbital energy
$^2F_{5/2}$	−240785.9763	−37.8243		
$^2F_{7/2}$	−240785.7206	−37.4979	−1001.6971	−37.5061
$^2D_{3/2}$	−240780.4928	−29.8901		
$^2D_{5/2}$	−240780.2208	−29.5936	−995.4003	−29.7992
$E_{^2D_{5/2}}-E_{^2F_{7/2}}$	5.4998		6.2995	

is treated as if it were a molecule, and the Hartree-Fock equations are solved only for this limited part of the crystal. To represent the interaction of the cluster with the rest of the lattice, it is surrounded with point charges, which are fitted to ensure the correct Madelung potential at the cluster sites.

In the G94 code, the Hartree-Fock formalism is formulated in the LCAO form with a fixed Gaussian basis set, which can be found in Ref. 10. For Ce^{3+}, we used the scalar relativistic effective core potential (ECP) of Stevens *et al.*,[11,12] with a $[Kr\ 4d^{10}]$ core, to describe the electron-ion interactions. To investigate the effect of using a basis set of Gaussians and an ECP for Ce^{3+}, we have first investigated the free Ce^{3+} ion with G94 and with the fully relativistic multiconfigurational Dirac-Fock (MCDF) code of Desclaux,[13] both at the Hartree-Fock level.

With the MCDF code we calculated the total energy of the Ce^{3+} ion in the $4f$ ground-state configuration ($[Xe]4f^1$), J multiplets $^2F_{5/2}$ and $^2F_{7/2}$, and of the $5d$ excited-state configuration ($[Xe]5d^1$), J multiplets $^2D_{3/2}$ and $^2D_{5/2}$. From these calculations we find a ΔSCF between the $^2D_{5/2}$ and $^2F_{7/2}$ multiplets of around 5.5 eV. The experimentally determined excitation energy between these Ce^{3+} states, taken from Ref. 14, is found to be ≈ 1 eV larger. This difference of 1 eV between the excitation energy, found in the MCDF calculations at the Hartree-Fock level, and as determined from experiment, is usually defined as the correlation energy.

Calculation of the total energy of the $^2F_{7/2}$ and $^2D_{5/2}$ multiplets of Ce^{3+}, using G94, gives an energy difference which is 0.80 eV larger than the result obtained with MCDF. To compensate for using a basis set of Gaussians and an ECP for Ce^{3+}, we will correct the ΔSCF, as calculated with G94, between a cluster containing Ce^{3+} in a $4f$ configuration and an identical cluster containing Ce^{3+} in a $5d$ configuration, by this amount. The results of the calculations on free Ce^{3+} are summarized in Table I.

On embedding Ce^{3+} in a solid, the *LS* term ^2D will be splitted by the crystal field and the fivefold degeneracy will be lifted in accordance with the symmetry of the site the ion occupies. To calculate the crystal-field splitting of the Ce^{3+} $5d$ configuration in a cluster of choice, we can follow either of two approaches: (i) The crystal-field splitting can be obtained from the ΔSCF energies between cluster calculations on Ce^{3+} with different $5d$ crystal-field states actually occupied by an electron, or (ii) the crystal-field splitting can be found from the differences between the orbital energies of the virtual $5d$ crystal-field states of Ce^{4+}.

Although in our experience results obtained following the second approach show good agreement with ΔSCF results, for Ce^{3+} in a range of different crystalline environments, and despite the fact that it is computationally cheaper to calculate the crystal-field splitting of the Ce^{3+} $5d$ manifold from Ce^{4+} virtual $5d$ crystal-field states, we prefer to work with ΔSCF results. Therefore, unless indicated otherwise, one may assume results on the crystal-field splitting of the Ce^{3+} $5d$ manifold, presented in this paper, to be obtained from ΔSCF energies.

In case of a strong cubic crystal-field splitting, spin-orbit interaction can be included as a second-order perturbation to the energy of the crystal-field states. The perturbation term due to spin-orbit interaction between two crystal-field states with energy E_n and E_m, respectively, is of the order of $\lambda^2/(E_n-E_m)$, where λ (≈ 0.12 eV) is the spin-orbit parameter of the $5d$ manifold of the free Ce^{3+} ion. (Often it will be considerably smaller, because delocalization of the Ce^{3+} $5d$ electron in the solid tends to quench the spin-orbit interaction.) In $LiBaF_3$, the Ce^{3+} $5d$ manifold shows a perturbed cubic crystal-field splitting. Spin-orbit interaction can mix states derived from the e level with states derived from the t_2 level, but all our calculations on Ce^{3+} in $LiBaF_3$ will show the crystal-field splitting between these states to be large compared to λ. Spin-orbit interaction can also mix the t_2 derived states $t_{2\zeta}(d_{xy})$, $t_{2\eta}(d_{xz})$, and $t_{2\xi}(d_{yz})$ with each other. Together with the crystal-field splitting this leads to a threefold splitting of the t_2 level for all cases we will consider in this paper. The decision whether or not to include spin-orbit interaction in our calculations will be made for each case presented in Sec. VI separately, based on a comparison of the calculated crystal-field splitting with the splitting of the Ce^{3+} $5d$ manifold found in optical-absorption measurements.

To calculate the energy of a certain $4f \rightarrow 5d$ absorption (or $5d \rightarrow 4f$ emission) line of Ce^{3+} in a given cluster, we take the ΔSCF between Ce^{3+} in the $^2F_{5/2}$ ground state and Ce^{3+} with an electron in the relevant $5d$ crystal-field state.

Besides the crystal-field splitting of the Ce^{3+} $5d$ configuration, experiments also show a decrease of the energy difference between the $5d$ and $4f$ centroids, of around 1–2 eV, with respect to the free ion value. For unknown reasons we do not obtain this decrease in our calculations with G94. However, in our experience the energy differences between

the $5d$ and $4f$ centroids, as calculated with G94, agree with experiment to within 0.1 eV for Ce^{3+} in a range of different fluorine crystals. It seems that the missing decrease in the $5d$-$4f$ centroid energy difference is almost completely compensated by the fact that we neglect effects of correlation in our calculations with G94.

As was shown above, the correlation energy of a free Ce^{3+} ion is close to 1 eV. Effects of correlation in Ce^{3+} are largely an aspect of its $4f$ electron. Embedding Ce^{3+} in a solid hardly affects this $4f$ electron, since it is shielded from the crystalline environment by the filled $5s$ and $5p$ shells of the ion. Therefore, it is reasonable to assume that the correlation energy of Ce^{3+} as a dopant ion will be close to the free ion value. This means that when we neglect to take correlation into account, the energy of a cluster containing Ce^{3+} in a $[Xe]4f^1$ configuration will be ≈ 1 eV too high with respect to the energy of an identical cluster, containing Ce^{3+} in a $[Xe]5d^1$ configuration. This indeed will almost completely compensate for the fact that our cluster calculations fail to reproduce the experimentally observed centroid shift of 1 eV in most Ce^{3+} doped fluorides.

III. GEOMETRY OPTIMIZATIONS

Previous work on the lattice relaxation in $LiBaF_3:Ce^{3+}$ was done using the pair-potential code HADESII,[15] and to a lesser extent using the possibilities of geometry optimization in the GAUSSIAN™ G94 program. The HADESII code calculates the relaxation and polarization of an essentially infinite lattice containing an impurity (complex). However, the interaction between the ions is given by semiempirical pair potentials, whose interaction parameters were not fitted to measurements on $LiBaF_3$ itself, but were taken from earlier work on LiF and BaF_2. The G94 program employs an *ab initio* description of the electron-electron and electron-ion interactions. However, optimizing the configuration of a system consisting of a defect complex and its nearest and next-nearest neighbors, i.e., a few tens of atoms, with respect to all ionic degrees of freedom, using G94, is prohibitively time consuming.

For our recent calculations of the lattice relaxation, we used the Vienna Ab initio Simulation Package (VASP).[16,17] The VASP program calculates the electronic ground state of a periodic system and the Hellmann-Feynman forces acting on the nuclei in its unit cell, within the framework of the DFT, using a plane-wave basis set to represent the electronic wave functions and pseudopotentials to describe the electron-ion interaction. The Hellmann-Feynman forces acting on the pseudoatoms in the unit cell are then used to minimize the free energy with respect to the ionic coordinates.

To approximate the case of an isolated luminescence center in a $LiBaF_3$ host lattice, we used the so-called supercell approach. In order to prevent the interaction between a luminescence center and its periodic images, the supercell must be large enough to contain the complete relaxation and polarization of the lattice, caused by the introduction of the luminescence center into the host. In the case of $LiBaF_3:Ce^{3+}$ this can easily become a problem because the luminescence centers we are considering consist of two defects, one with a positive and one with a negative effective charge, separated by distances of the order of the nearest-neighbor bond lengths and larger. These defect complexes may have quite a large dipole moment, leading to considerable dipole-dipole interaction between the defects and their periodic images, especially in highly ionic materials such as $LiBaF_3$ that exhibit an incomplete dielectric screening of electrostatic interactions.

The relaxation studies presented here were all done on a simple cubic supercell made up of $3\times3\times3$ unit cells of $LiBaF_3$, containing a single luminescence center. Optimizing the geometry of a supercell of this size, containing around 135 atoms, is computationally very demanding. This puts serious limitations on the number of points in the sampling of the Brillouin zone and on the possibility to check the results for convergence with respect to an increase in the size of the supercell. The sampling of the BZ was limited to a single point, the Γ point, and convergence with respect to supercell size could only be checked by comparison with calculations on supercells smaller than $3\times3\times3$ unit cells, e.g., a $2\times2\times3$ supercell.

We used Vanderbilt-type[18] ultrasoft pseudopotentials (USPP), supplied by the Institute für Theoretische Physik of the Technische Universität Wien,[19] with frozen [He] cores for Li and F, and a $[Kr\ 5s^2 4d^{10}]$ core in the case of Ba.

For Ce we made use of two different pseudopotentials. The USPP, hereafter labeled Ce, was generated from a $[Kr\ 5s^2 4d^{10} 4f^1] 5p^6 5d^1 6s^2$ electronic configuration. This pseudopotential was used to describe the $[Xe]4f^1$ ground-state electronic configuration of Ce^{3+}. The single $4f$ electron of Ce in the ground state was put in the core of the pseudopotential. It might seem strange to treat the $4f$ electron, which is the least strongly bound electron in a Ce^{3+} ion, as a core electron. However, the $4f$ electron is strongly localized, and the maximum of the radial part of its wave function is found quite a bit closer to the nucleus than the maxima of the $5s$ and $5p$ wave functions. Consequently, the filled $5s$ and $5p$ orbitals of Ce^{3+} make up the outside of the ion and tend to shield the $4f$ electron from the crystalline environment. Therefore, in matters concerning the chemical bonding of Ce^{3+} as a dopant ion in an ionic material, it is justified to include its $4f$ electron in the core of the pseudopotential. Furthermore, treating the $4f$ electron as a valence electron tends to yield unphysical results, due to its large spurious self-interaction within the LDA.

The USPP, hereafter denoted Ce*, was generated from a $[Kr\ 5s^2 4d^{10}] 5p^6 5d^2 6s^2$ electronic configuration. It lacks the single $4f$ electron in its core and contains no component of angular momentum $l=3$. This pseudopotential represents the Ce^{3+} ion in the $[Xe]5d$ excited-state configuration and was used to study the relaxation of the lattice, induced by a Ce^{3+} $4f \rightarrow 5d$ excitation.

We employed kinetic energy cutoffs of, respectively, 272.5 eV and 1500 eV, for the plane-wave basis sets which are used to represent the wave functions and the augmentation charge density.

Exchange and correlation were treated in the generalized gradient approximation (GGA), based on the parametrization by Perdew and Zunger[20] of the local-density functional of Ceperley and Alder,[21] with the gradient corrections following Perdew and Wang[22] (PW91).

The solution to the generalized Kohn-Sham equations was calculated using a matrix diagonalization routine based on

the sequential iterative optimization of each band using a preconditioned conjugate-gradient algorithm and a modified Broyden charge-density mixing.[17]

We used a Gaussian smearing of the Fermi surface, with a width of 0.01 eV. Since $LiBaF_3$ is a wide-band-gap insulator, normally the results would be insensitive to the width of the Fermi-surface smearing. This is true for the calculations on supercells containing Ce^{3+} in the $4f$ configuration. However, in the case in which we study the relaxation of the lattice around Ce^{3+} in its $5d$ configuration, we aim to populate only the first $5d$ crystal-field state above the valence band. (Excitation of Ce^{3+} into higher-lying states within the $5d$ manifold would in reality be followed by a rapid nonradiative deexcitation to the lowest $5d$ crystal-field state.) This state potentially lies close in eigenenergy to the other Ce^{3+} crystal-field states or to states belonging to the conduction band. The small width of the Gaussian smearing is chosen to ensure that the lowest state in the Ce^{3+} $5d$ manifold is populated by one electron.

The relaxation of the ions into their instantaneous ground state was done using a conjugate-gradient, predictor/corrector-type algorithm.[17] All nonlocal contributions to the Hamiltonian and Hellmann-Feynman forces were calculated in reciprocal space.

IV. STOKES SHIFT

The Stokes shift is found from experiment as the energy difference between the Ce^{3+} $4f \rightarrow 5d$ absorption line, corresponding to a transition from the $^2F_{5/2}$ ground state to the lowest $5d$ crystal-field state, and the average of the two Ce^{3+} $5d \rightarrow 4f$ emission lines, corresponding to transitions from the lowest $5d$ crystal-field state to the $^2F_{7/2}$ and $^2F_{5/2}$ J multiplets of the spin-orbit splitted ground state.

In $LiBaF_3$:Ce^{3+} this is the energy difference between the absorption line at 250 nm and the peak of the emission band at 320 nm, i.e., approximately 1 eV.

The origin of the Stokes shift is explained easiest by way of the *single configurational coordinate model* depicted in Fig. 1. This configuration diagram shows the sum of the electronic energy and the potential energy of the ions in a system containing Ce^{3+} in its ground state and in a system containing Ce^{3+} in its first excited state, curves labeled $4f$ and $5d$, respectively, as a function of the generalized configurational coordinate Q, which can be made up of any relevant combination of ionic degrees of freedom in the system. The horizontal lines inside the curves $4f$ and $5d$ denote phonon states of the system, i.e., they are lines of constant total energy. In general, the equilibrium configuration of the system will depend on the electronic configuration of the Ce^{3+} ion. This is represented in Fig. 1 by the difference between Q_{01} and Q_{02}, the equilibrium values of the configurational coordinate, for the system with Ce^{3+} in its ground state and its excited state, respectively. After excitation of the Ce ion, $E_0 \rightarrow E_1$, the system will be out of thermal equilibrium, and will relax from configuration Q_{01} towards Q_{02}. Following the radiative transition of Ce^{3+} from its excited state to the ground state, $E_2 \rightarrow E_3$, the system will again be out of thermal equilibrium, and will relax from Q_{02} back to the initial configuration Q_{01}. From the configuration diagram of Fig. 1 we then find a Stokes shift of

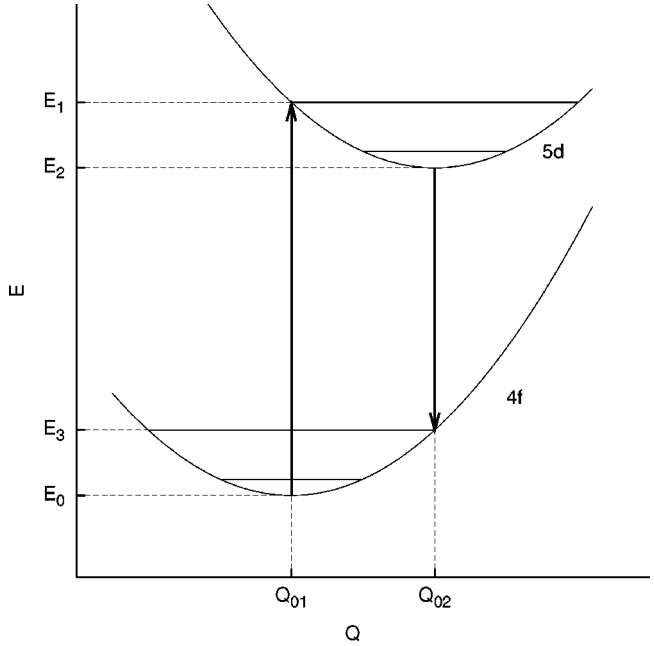

FIG. 1. The single configurational coordinate model.

$$\Delta E_{\text{Stokes}} = (E_1 - E_0) - (E_2 - E_3). \quad (1)$$

We find the Stokes shift both from cluster calculations with G94 as well as from supercell calculations with VASP. Using VASP we first optimize the geometry of a supercell, containing Ce^{3+} in its ground state, as part of the luminescence center. This gives the coordinates (Q_{01}, E_0) in configurations space. We then substitute Ce^{3+} with $(Ce^{3+})^*$ and calculate the lattice relaxation, $Q_{01} \rightarrow Q_{02}$, induced by this excitation. The first and last iterations of this calculation provide, respectively, (Q_{01}, E_1) and (Q_{02}, E_2). To find (Q_{02}, E_3) we then replace $(Ce^{3+})^*$ with Ce^{3+} in geometry Q_{02} and minimize the total energy with respect to the electronic degrees of freedom only.

Once the geometries Q_{01} and Q_{02} are known from the supercell optimizations with VASP, it is also possible to find the Stokes shift from cluster calculations with G94. From both geometries we take a cluster, Q'_{01} and Q'_{02}, respectively, and generate the corresponding arrays of point charges to represent the rest of the crystal. On each cluster we do two calculations, one with Ce^{3+} in the $^2F_{5/2}$ ground state and one for Ce^{3+} in its lowest $5d$ crystal-field state. From the calculations on Q'_{01} we find (Q'_{01}, E_0) and (Q'_{01}, E_1). The ΔSCF value, $E_1 - E_0$, should be equal to the energy of the lowest Ce^{3+} $4f \rightarrow 5d$ absorption line found from experiments. From the calculations on Q'_{02} we find (Q'_{02}, E_3) and (Q'_{02}, E_2), where $E_2 - E_3$ corresponds to the energy of the Ce^{3+} $5d \rightarrow 4f$ emission, from the lowest $5d$ crystal-field state to the $^2F_{5/2}$ ground state.

V. RELIABILITY OF THE APPROACH

Wherever possible we have tried to check the results of calculations with G94 against calculations with VASP and vice versa. We consider this to be essential, because the nature of both these calculational methods is such that, without intercomparison, it is in many cases impossible to identify

artifacts in the results, introduced by the respective methods, or to give an estimate of the systematic errors.

Although, as was mentioned before, it is not tractable to use G94 to optimize the geometry of a system consisting of several tens of atoms, there are some possibilities to use it to check parts of the optimized geometries obtained with VASP. This is done by investigating the structural stability of a cluster of atoms, taken from the equilibrium structure predicted by VASP. To determine whether a cluster is stable with respect to changes in a generalized coordinate, q_i, we calculate the first and second derivatives of its total energy $E^{(1)} = \partial E/\partial q_i$ and $E^{(2)} = \partial^2 E/\partial q_i^2$. From this we find a prediction of the displacement along this coordinate, towards the equilibrium structure of the cluster, of $\Delta q_i = -E^{(1)}/E^{(2)}$. This approach has three major drawbacks. (i) It is only exact in case the total energy depends quadratically on q_i, where q_i represents a normal mode of the cluster. (ii) Only coordinates involving displacements of atoms, whose complete shells of nearest neighbors are included in the cluster, can be investigated. For atoms at the edge of the cluster, part of the repulsive interaction with their surroundings is missing, and predicted displacements will be unphysical. (iii) Checking the stability of the cluster with respect to a single coordinate requires three full SCF calculations to determine the second derivative $\partial^2 E/\partial q_i^2$.

Despite these drawbacks, G94 still provides a very useful check on the results of the supercell calculations, especially with respect to errors due to the application of periodic boundary conditions in the supercell method, e.g., due to possible interaction between periodic images and the limited sampling of the Brillouin zone.

Our options to use VASP, to check the G94 calculations on the Ce^{3+} absorption and emission lines, are fairly limited, since it is impossible to realistically treat a $4f$ electron as a valence electron within the LDA. It is, however, possible to determine the splitting of the Ce^{3+} $5d$ manifold from calculations with VASP and to compare this splitting and the orbital ordering with those found with G94. This is done by populating the first five states above the valence band with 0.2 electrons each. These occupation numbers are kept fixed during the subsequent minimization of the total energy with respect to the electronic degrees of freedom. If inspection of the site-projected density of states shows that the resulting five partially occupied states above the valence band are dominantly made up of *d* character at the Ce site, then these states make up the crystal-field-splitted Ce^{3+} $5d$ manifold. From the differences between the eigenenergies of these states, we then find the predicted splitting of the Ce^{3+} $4f \rightarrow 5d$ absorption lines.

VI. RESULTS

A. Pure $LiBaF_3$

We will first discuss the electronic structure of pure $LiBaF_3$, as calculated with VASP. First the self-consistent charge density in a primitive cell of $LiBaF_3$ was determined, using a $4\times4\times4$ Monkhorst-Pack[23] **k**-point mesh. This charge density was kept constant during the subsequent calculation of the eigenvalues of the bands at 100 **k** points along lines of high symmetry in the Brillouin zone. The band structure and corresponding density of states of $LiBaF_3$ are shown in Fig. 2. The bands around -24.5 and -14.0 eV are derived from F $2s$ and Ba $5p$ states, respectively. The Fermi level is found at -5.3723 eV, which coincides with the top of the valence band, since $LiBaF_3$ is an insulator. The valence band has a width of 3.5 eV and is made up of F $2p$ states. The bottom of the conduction band, above 1.2795 eV, is primarily derived from Ba $5d$ (e_g) states. We find a direct gap, of 6.65 eV, between the top of the valence band and the bottom of the conduction band at Γ. The size of the gap is too small compared to the experimentally determined value of $\approx$10.2 eV (Ref. 24). This underestimation of the band gap is a common deficiency of calculational methods which make use of the local-density approximation (LDA). The exchange-correlation energy in the LDA lacks the required discontinuity at the Fermi energy and the LDA suffers from spurious self-interaction, resulting in a positioning of the valence bands at higher energies. The effects of these shortcomings of the LDA on the conduction bands are much less pronounced, since these bands are unoccupied, which leads to the observed underestimation of the band gap.

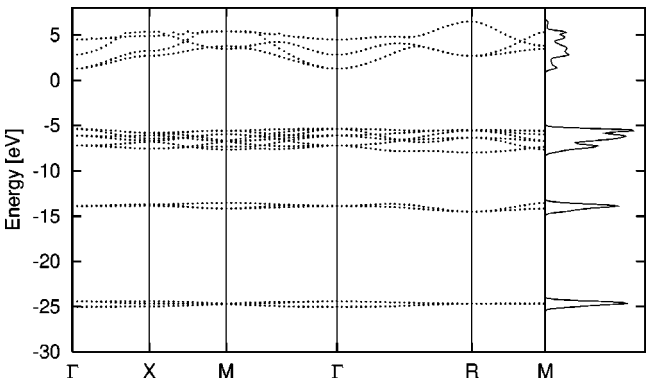

FIG. 2. The band structure and corresponding DOS (right-hand side panel) of $LiBaF_3$, calculated with VASP.

B. Ce^{3+} on a Ba site + a vacancy at a nearest Li site

To determine the equilibrium configuration of this luminescence center, we optimized the geometry of a $3\times3\times3$ supercell of $LiBaF_3$ (see Sec. III), in which one Ba ion was substituted by a Ce ion and one of the Li ions nearest to the Ce substitution was removed. The relaxed structure has a total energy of $-717.003\,27$ eV. The lattice relaxation remains largely limited to displacements of the Ce ion, its twelve nearest-neighboring F ions, and the seven next-nearest-neighboring Li ions. This section of the optimized supercell geometry is shown in Fig. 3. The symmetry of the Ce site remains C_{3v}. The Ce ion has moved $\approx$0.17 Å along a $\langle 111\rangle$ direction, towards the Li vacancy. The twelve nearest-neighboring F ions have moved towards the Ce ion. The largest displacements, of $\approx$0.27 Å, are those of the three F ions found at $\langle \frac{1}{2}\,0\,0\rangle$ directions with respect to the Li vacancy. The groups of F ions, found at $\langle \frac{1}{2}\,1\,0\rangle$ and $\langle \frac{1}{2}\,1\,1\rangle$ directions with respect to the Li vacancy, respectively, show displacements of 0.15 and 0.1 Å. The next-nearest-neighboring Li ions have moved slightly outward, away from the Ce substitution, none, however, more than 0.05 Å.

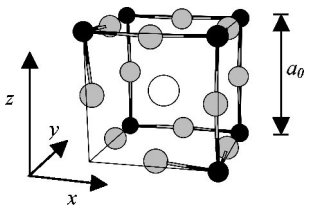

FIG. 3. Part of the $3\times3\times3$ $LiBaF_3$ supercell containing a Ce substitution on a Ba site plus a vacancy at a nearest Li site, after relaxation. The cerium, fluorine, and lithium ions are depicted as, respectively, white, gray, and black circles.

From the supercell configuration, of which part is depicted in Fig. 3, we took a cluster of atoms, consisting of the Ce ion plus its shells of nearest and next-nearest neighbors, i.e., respectively, 12 F and 7 Li ions. Table II contains the positions of the atoms in this cluster, given in Cartesian coordinates. From calculations on this cluster geometry, we find the Ce^{3+} $4f\rightarrow5d$ absorption lines, as outlined in Sec. II. The results of these calculations and the experimentally determined absorption lines are listed in Table III.

As can be clearly seen, the main disagreement between the predicted and the observed Ce^{3+} $4f\rightarrow5d$ transitions consists in the fact that calculations predict a threefold splitting of the Ce^{3+} $5d$ manifold whereas four $4f\rightarrow5d$ absorption bands are observed. Contrary to what was speculated on in Sec. I, also after relaxation has been taken into account for this luminescence center configuration, the lowest Ce^{3+} $5d$ crystal-field state consists of the twofold degenerate cubic e level. No attempt was made to include the effects of spin-orbit coupling since, as was briefly mentioned in Secs. I and II, the cubic e level will not be split up by the spin-orbit interaction. Spin-orbit coupling will lift the remaining degeneracy in the t_2 derived states, but not to an extend that is likely to lead to better agreement between calculation and experiment insofar as the missing absorption line at 5.166 eV is concerned.

TABLE II. $CeF_{12}Li_7$ cluster, representing the luminescence center consisting of Ce^{3+} on a Ba site, charge compensated by a vacancy at one of the nearest Li sites (all coordinates are in Å).

Ion	x	y	z
Ce	0.00000	0.00000	0.00000
Li	−1.87117	−1.87117	2.10207
Li	−1.86758	2.07695	2.07695
Li	2.07815	−1.86758	2.07695
Li	2.06618	2.06499	2.06618
Li	2.10207	−1.87117	−1.87117
Li	−1.87117	2.10207	−1.87117
Li	2.07815	2.07695	−1.86758
F	0.11485	−1.77905	1.99679
F	−1.77905	0.11366	1.99679
F	0.10289	2.01713	2.01713
F	2.01833	0.10169	2.01833
F	0.18544	−1.74315	−1.74196
F	−1.74196	0.18544	−1.74196
F	0.11485	1.99679	−1.77905
F	1.99799	0.11366	−1.77905
F	−1.74196	−1.74315	0.18544
F	−1.77905	1.99679	0.11366
F	1.99799	−1.77905	0.11366
F	2.01833	2.01713	0.10289

TABLE III. The Ce^{3+} $4f\rightarrow5d$ absorption lines, as calculated from a $CeF_{12}Li_7$ cluster, representing a luminescence center consisting of Ce^{3+} on a Ba site, charge compensated by a vacancy at one of the nearest Li sites.

State	HF energy (eV)	$4f\rightarrow5d$ (eV)	
		Predicted	Observed
$^2F_{5/2}$	−66683.72310		
$5d(e_g)$ (2×)	−66677.85397	5.06945	4.960
			5.166
$5d(t_2)$	−66677.16744	5.75598	5.688
$5d(t_2)$ (2×)	−66676.94440	5.97902	6.078

C. Ce^{3+} on a Li site + a vacancy at a nearest Ba site

To determine the equilibrium configuration of this luminescence center, we optimized the geometry of a $3\times3\times3$ supercell of $LiBaF_3$ (see Sec. III), in which one Li ion was substituted by a Ce ion and one of the Ba ions nearest to the Ce substitution was removed. The relaxed structure has a total energy of −713.355 91 eV. The lattice relaxation remains largely limited to displacements of the nearest and next-nearest neighbors of the Ba vacancy, i.e., respectively, twelve F ions and the Ce ion plus seven Li ions. This section of the optimized supercell is shown in Fig. 4. Again the symmetry of the Ce site remains C_{3v}. The largest displacements are those of the Ce ion and the three F ions which are nearest neighbors to both the Ce substitution, as well as to the Ba vacancy. The Ce ion has moved ≈0.55 Å along a ⟨111⟩ direction, towards the Ba vacancy. The beforementioned F ions have moved radially outward with respect to the Ba vacancy by 0.17 Å and away from the Ce ion towards their Li nearest neighbors by 0.36 Å. The other three F nearest neighbors of the Ce substitution remain more or less at their regular lattice sites.

From the supercell configuration, of which part is depicted in Fig. 4, we took a cluster, consisting of the Ce ion plus two shells of neighbors, consisting of six F and six Li ions. Table IV contains the positions of the atoms in this cluster, given in Cartesian coordinates. From calculations on this cluster geometry, we find the Ce^{3+} $4f\rightarrow5d$ absorption

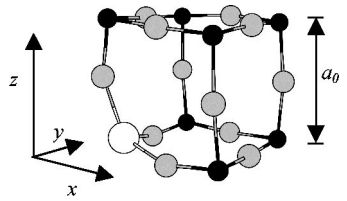

FIG. 4. Part of the $3\times3\times3$ $LiBaF_3$ supercell containing a Ce substitution on a Li site plus a vacancy at a nearest Ba site, after relaxation. The cerium, fluorine, and lithium ions are depicted as, respectively, white, gray, and black circles.

TABLE IV. CeF_6Li_6 cluster, representing the luminescence center consisting of Ce^{3+} on a Li site, charge compensated by a vacancy at one of the nearest Ba sites (all coordinates are in Å).

Ion	x	y	z
Ce	0.00000	0.00000	0.00000
Li	−0.31106	−0.31106	3.83087
Li	−0.29551	−0.29551	−4.33216
Li	−0.31106	3.83087	−0.31106
Li	−0.29551	−4.33216	−0.29551
Li	3.83087	−0.31106	−0.31106
Li	−4.33216	−0.29551	−0.29551
F	−0.51804	−0.51804	2.03149
F	−0.28355	−0.28355	−2.29470
F	2.03149	−0.51804	−0.51804
F	−0.51804	2.03029	−0.51804
F	−0.28355	−2.29470	−0.28355
F	−2.29470	−0.28355	−0.28355

lines, as outlined in Sec. II. The results of these calculations and the experimentally determined absorption lines are listed in Table V.

The extend of the splitting of the Ce^{3+} $5d$ manifold is more than three times larger than experimentally observed. Since disagreement with experiment of this magnitude will surely not be solved by taking spin-orbit interaction into account, again no attempt was made to do so.

D. Ce^{3+} at a Ba site + Li^{+} at a nearest Ba site

1. Supercell calculations

Ce^{3+} ground state. To determine Q_{01} (see Sec. IV), the equilibrium configuration of this luminescence center, we optimized the geometry of a $3\times3\times3$ supercell of $LiBaF_3$ (see Sec. III), in which one Ba ion was substituted by a Ce ion, and where a Li ion occupied one of the Ba sites nearest to the Ce substitution. Part of this supercell, containing both substitutions, is shown in Fig. 5. Our calculations predict two different equilibrium configurations of the luminescence center, resulting after relaxation of the lattice, labeled Q_{01a} and Q_{01b}. These are shown, again in part, in Figs. 6(a) and 6(b), respectively.

Both resulting configurations show the Ce ion to move along the z axis, towards the Li substitution, by ≈0.23 Å.

TABLE V. The Ce^{3+} $4f\rightarrow5d$ absorption lines, as calculated from a CeF_6Li_6 cluster, representing a luminescence center consisting of Ce^{3+} on a Li site, charge compensated by a vacancy at one of the nearest Ba sites.

State	HF energy (eV)	$4f\rightarrow5d$ (eV)	
		Predicted	Observed
$^2F_{5/2}$	−52599.65077		
$5d(t_2)$ (2×)	−52594.86302	3.98806	4.960
$5d(t_2)$	−52594.18003	4.67106	5.166
			5.688
$5d(e_g)$ (2×)	−52591.51171	7.33938	6.078

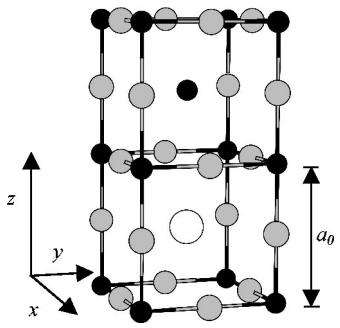

FIG. 5. Part of the $3\times3\times3$ $LiBaF_3$ supercell containing a Ce and a Li substitution on neighboring Ba sites, before lattice relaxation. The cerium, fluorine, and lithium ions are depicted as, respectively, white, gray, and black circles.

The F ions in the $z=0$ and $z=\frac{1}{2}a_0$ move ≈0.13 Å inwards, in the direction of the Ce ion. The four F ions in the $z=a_0$ plane, between the substitutional Li ion and the Ce ion, move away from the charge-compensating defect towards the Ce ion by ≈0.22 Å. Movement away from the Li substitution is also shown by the other F ions which surround it. These displacements are a result of the electrostatic forces between the negatively charged F ions and the respective positive and negative effective charges of the Ce^{3+} and Li^{+} substitutions on Ba^{2+} sites.

The two possible configurations, Q_{01a} and Q_{01b}, resulting after relaxation, differ mainly with respect to the displacement of the substitutional Li ion. In both cases the Li ion moves away from the nominal Ba site by ≈1.1 Å. However, where configuration Q_{01a} shows the Li ion to move upwards along the z axis, and to end up nested against the four F ions in the plane above it, configuration Q_{01b} shows the Li ion to move along a ⟨111⟩ direction, ending up in a corner between three F ions. The latter equilibrium position of the Li ion is of course fourfold degenerate, in the sense that there are four ⟨111⟩ directions along which the Li ion could have moved. The two equilibrium configurations, Q_{01a} and Q_{01b}, have almost the same total energy, respectively, −719.390 93 and −719.405 83 eV.

This indicates that, at room temperature, the substitutional Li ion may have a considerable mobility in the area between

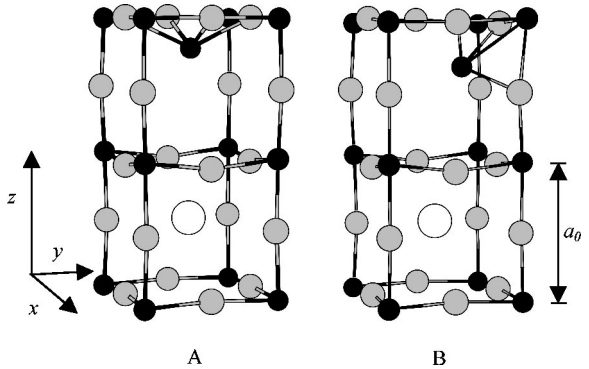

FIG. 6. Part of the $3\times3\times3$ $LiBaF_3$ supercell containing a Ce and a Li substitution on neighboring Ba sites, after lattice relaxation. (a) Li has moved along a ⟨100⟩ direction. (b) Li has moved along a ⟨111⟩ direction. The cerium, fluorine, and lithium ions are depicted as, respectively, white, gray, and black circles.

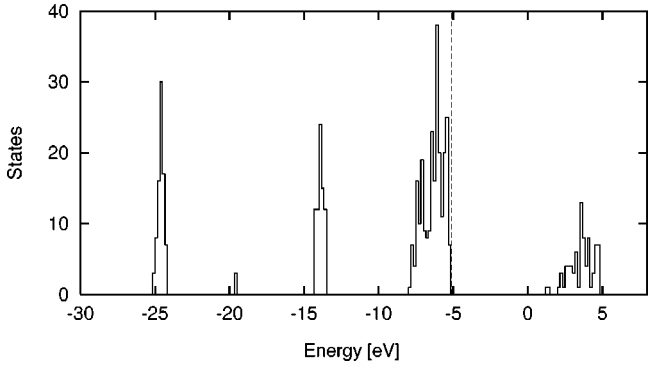

FIG. 7. Histogram (bin size=0.16 eV) of the density of states in the supercell with configuration Q_{01a}, in the Γ point. The dashed line indicates the position of the Fermi energy.

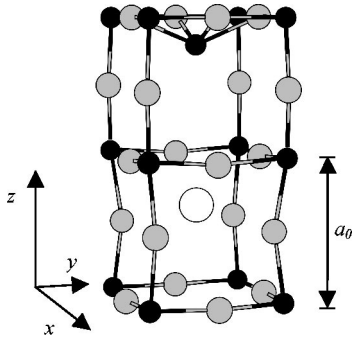

FIG. 8. Part of the $3\times3\times3$ $LiBaF_3$ supercell containing a Ce and a Li substitution on neighboring Ba sites, after the lattice relaxation induced by the Ce→Ce* excitation. The cerium, fluorine, and lithium ions are depicted as, respectively, white, gray, and black circles.

its different equilibrium positions. In the following we will not take the different equilibrium positions of the substitutional Li ion into account, but we will limit ourselves to the Q_{01a} configuration.

Figure 7 shows the density of states at Γ, in the supercell with configuration Q_{01a}. Compared to the density of states in pure $LiBaF_3$, depicted in Fig. 2, the positions of the F $2s$, Ba $5p$, and F $2p$ derived bands remain unaltered. The band around -19.5 eV is derived from Ce $5p$ states. The Fermi level is found at -5.2722 eV, again coinciding with the top of the F $2p$ derived valence band. The bottom of the conduction band is found around 1.29 eV. On the whole, the conduction band is mainly derived from Ba $5d$ states. However, sizable admixture of Ce $5d$ character into the Ba $5d$ derived states is present throughout the lower part of the conduction band, up to 3 eV. Notably the first states above the valence band, at 1.293 63 and 1.370 65 eV, are derived from, respectively, mixed Ce + Ba $5d_{z^2}$ and $5d_{x^2-y^2}$ states.

Ce^{3+} excited state. To predict the splitting of the Ce^{3+} $4f\rightarrow5d$ absorption lines observed in experiment, we performed a calculation on the excited state of Ce^{3+} in configuration Q_{01a}, as outlined in Sec. V. The five partially occupied states above the valence band are indeed found to be dominantly made up of d character at the Ce site. The dominant orbital character, energy, and both the predicted as well as the experimentally observed splitting of the levels in the Ce^{3+} $5d$ manifold are listed in Table VI.

The lattice relaxation following the $Ce^{3+}\rightarrow(Ce^{3+})^*$ excitation starts from the configuration Q_{01a} [see Fig. 6(a)], at a total energy of $-717.887\,05$ eV. The resulting configuration after relaxation, Q_{02} (see Sec. IV), shown in Fig. 8, has a total energy of $-718.107\,57$ eV. This relaxation is dominated by the movement of the Ce ion and its nearest-neighboring F ions in the $z\approx\frac{1}{2}a_0$ plane. The Ce ion moves along the z axis, towards the substitutional Li ion, by ≈0.38 Å. The F ions in the $z\approx\frac{1}{2}a_0$ plane move inwards ≈0.25 Å, along $\langle110\rangle$ directions to within 2.67 Å of the Ce ion, while the F ions in the $z\approx a_0$ plane move outwards ≈0.15 Å, in the direction of their nominal positions in unperturbed $LiBaF_3$.

TABLE VI. The splitting of the Ce^{3+} $5d$ manifold in geometry Q_{01a}, as calculated with VASP from the eigenenergies of the first five states above the F $2p$ derived bands. The occupation numbers of these states were set to 0.2 electrons and were kept fixed.

Eigenenergy (eV)	Dominant character	Splitting (eV)	
		Predicted	Observed
0.55727	$5d_{z^2}$	0.0	0.0
0.80355	$5d_{x^2-y^2}$	0.24628	0.206
1.24585	$5d_{xy}$	0.68858	0.728
1.49359	$5d_{yz}$	0.93632	1.118
1.50082	$5d_{xz}$	0.94355	

Figure 9 shows the density of states at Γ, in the supercell with configuration Q_{02}. The position and width of the F $2s$, Ba $5p$, and F $2p$ derived bands remain more or less unaltered, compared to the density of states in the supercell with configuration Q_{01a}, containing Ce in the ground state (see Fig. 7).

The Ce $5p$ derived states are now found around -21.5 eV. Since these states are largely localized on the Ce ion, they are shifted to lower energies due to the removal of the $4f$ electron from the core of the Ce pseudopotential.

The states around -25.6 and -8.37 eV, seemingly split off from, respectively, the F $2s$ and F $2p$ derived bands, are localized on the F ligands of the Ce ion, in the $z\approx\frac{1}{2}a_0$ and $z\approx a_0$ planes (see Fig. 8). These states are characterized by bonding combinations of, respectively, the Ce $5p$ + ligand F $2s$, and the Ce $5d_{xy}$ + ligand F $2p$ orbitals.

The Fermi level is found at 0.7045 eV, coinciding with the highest occupied state. The wave function of this singly

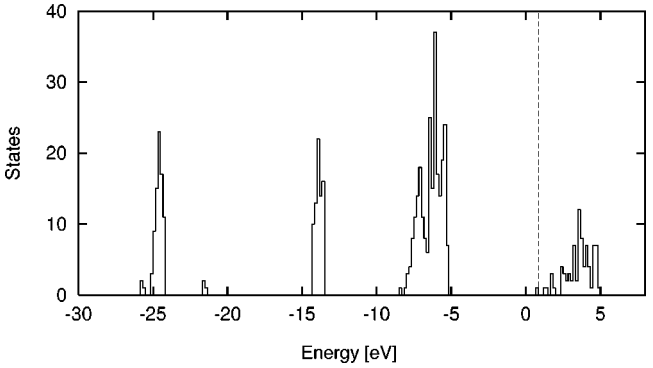

FIG. 9. Histogram (bin size=0.16 eV) of the density of states in the supercell with configuration Q_{02}, in the Γ point. The dashed line indicates the position of the Fermi energy.

TABLE VII. Total energies and character of the highest occupied state, as found in supercell calculations on the luminescence center consisting of Ce^{3+} on a Ba site, charge compensated by a Li at one of the nearest Ba sites, both for Ce^{3+} in the $[Xe]4f^1$ ground-state configuration as well as for its $[Xe]5d^1$ excited-state configuration, and each for both supercell geometry Q_{01a} as well as for geometry Q_{02}. Note that for Ce* in geometry Q_{01a} both the first as well as the second $5d$ crystal-field state could be found from total energy calculations.

Ce PP	Total energy (eV)	Character
	Configuration Q_{01a}	
Ce	−719.39093	F $2p$
Ce*	−717.88705	Ce $5d_{z^2}$
Ce*	−717.63888	Ce $5d_{x^2-y^2}$
	Configuration Q_{02}	
Ce	−719.13860	F $2p$
Ce*	−718.10757	Ce $5d_{z^2}$

occupied state is centered on the Ce ion, and almost completely localized in space between its twelve nearest neighboring F ions, the substitutional Li ion, and the Ba site below Ce. The site-projected density of states shows it to be characterized by an antibonding combination of the Ce $5d_{z^2}$ orbital and F $2p$ ligand orbitals. This state constitutes the lowest $5d$ crystal-field state of Ce^{3+} in $LiBaF_3$.

The bottom of the conduction band is again found around 1.29 eV. The conduction band is derived mainly from Ba $5d$ states. However, between 1.29 and 2 eV there is a sizable contribution of Ce $5d$ character in the conduction band.

Stokes shift. To find the Stokes shift of Ce^{3+} in $LiBaF_3$, one additional point in configuration space, (Q_{02},E_3) (see Sec. IV), corresponding to the total energy of a supercell with configuration Q_{02} containing Ce^{3+} in the ground state, was calculated. The results relevant to the calculation of the Stokes shift are listed in Table VII. From these total energies we find a Stokes shift of 0.472 85 eV.

2. Cluster calculations

From the supercell configurations, Q_{01a}, Q_{01b}, and Q_{02}, we took clusters of atoms, labeled Q'_{01a}, Q'_{01b}, and Q'_{02}, respectively (see Sec. IV), consisting of the Ce ion, its first, second, and third nearest neighbors (respectively 12 F, 8 Li, and 17 Ba ions), and the substitutional Li ion.

Cluster Q'_{01a} and Q'_{01b}. These clusters represent the equilibrium configuration of the lattice and luminescence center, when the Ce^{3+} ion is in its ^2F ground state. We checked the stability of these clusters, as described in Sec. III, with respect to displacements of the Ce ion, and its twelve neighboring F ions. The predicted displacements do not exceed 0.01 Å. Table VIII contains the positions of the atoms in the cluster Q'_{01a}, given in Cartesian coordinates.

From calculations on cluster Q'_{01a}, we find the energy of the Ce^{3+} $4f\rightarrow 5d$ absorption lines, as outlined in Sec. II. The results of these calculations and the experimentally determined absorption lines are listed in Table X. The lowest Ce^{3+} $5d$ crystal-field state is found to be dominantly made up of the $5d_{z^2}$ orbital.

TABLE VIII. Q'_{01a}, the $CeF_{12}Li_9Ba_{17}$ cluster, representing the luminescence center consisting of Ce^{3+} (in its ground-state configuration) on a Ba site, charge compensated by a Li at one of the nearest Ba sites (all coordinates are in Å).

Ion	x	y	z
Ce	0.00000	0.00000	0.00000
Li	−1.93697	−1.95372	1.79340
Li	−1.93936	1.95013	1.79340
Li	1.95252	−1.94774	1.79819
Li	1.95611	1.94774	1.79221
Li	−1.95851	1.97286	−2.18822
Li	−1.95611	−1.96927	−2.18702
Li	1.98363	−1.97047	−2.18822
Li	1.98483	1.97047	−2.18582
Li	0.04905	−0.04786	4.85858
F	0.00718	−1.89869	1.57087
F	−1.88313	−0.00359	1.57805
F	1.88792	−0.00359	1.57087
F	0.00837	1.90945	1.56968
F	−1.88074	−1.89629	−0.23569
F	−1.88433	1.90945	−0.23569
F	1.93219	−1.91065	−0.23330
F	1.93219	1.91663	−0.23569
F	0.01196	−1.90347	−2.10447
F	−1.89988	−0.00120	−2.10806
F	0.01077	1.91663	−2.10806
F	1.93697	−0.00598	−2.10925
Ba	0.00837	3.89069	3.73995
Ba	3.91223	−0.00120	3.74114
Ba	0.00837	−3.91582	3.73995
Ba	−3.89189	−0.00359	3.73875
Ba	0.01077	4.00076	−0.23928
Ba	4.00794	−0.00120	−0.23449
Ba	3.98880	3.97683	−0.22492
Ba	0.01436	−4.00435	−0.23928
Ba	3.98880	−3.98162	−0.22133
Ba	−3.99239	0.00000	−0.23689
Ba	−3.97205	3.97803	−0.22612
Ba	−3.97085	−3.98521	−0.22612
Ba	0.01077	0.00239	−4.10485
Ba	0.01316	3.96726	−4.22808
Ba	3.98282	−0.00120	−4.22329
Ba	0.01316	−3.98042	−4.22688
Ba	−3.96128	0.00000	−4.22568

Cluster Q'_{02}. This cluster represents the equilibrium configuration of the lattice and luminescence center after relaxation of the lattice, induced by the excitation of Ce^{3+} from the ground state to the $5d_{z^2}$ crystal-field state. Again the stability of the cluster was checked, with respect to displacements of the Ce ion and its twelve neighboring F ions. The largest predicted displacements, of ≈ 0.03 Å, were found for the F ions in the $z\approx a_0$ plane. These displacements were applied and Table IX contains the resulting positions of the atoms in the cluster Q'_{02}, given in Cartesian coordinates.

From calculations on cluster Q'_{02}, we find the energy of the Ce^{3+} $5d_{z^2}\rightarrow {}^2F$ emission line. The results of these cal-

TABLE X. The Ce^{3+} $4f \rightarrow 5d$ absorption lines. All results were found from calculations on a cluster with geometry Q'_{01a}.

State	HF energy (eV)	$4f \rightarrow 5d$ (eV)	
		Predicted	Observed
$^2F_{5/2}$	−98805.02351		
$5d_{z^2}$	−98799.33735	4.88648	4.960
$5d_{x^2-y^2}$	−98798.98236	5.24147	5.166
$5d_{xy}$	−98798.73125	5.49258	5.688
$5d_{xz}$,$5d_{yz}$	−98798.34507	5.87876	6.078

culations and the experimentally determined emission line are listed in Table XI.

Stokes shift. From the energy difference between the $^2F_{5/2} \rightarrow 5d_{z^2}$ absorption line, listed in Table X, and the $5d_{z^2} \rightarrow {}^2F_{5/2}$ emission line, stated in Table XI, we find a Stokes shift of 0.607 27 eV.

VII. SUMMARY AND CONCLUSIONS

A. The configuration of the luminescence center in $LiBaF_3$:Ce^{3+}

In this paper we studied the geometry and the electronic structure of three possible luminescence center configurations, consisting of a Ce^{3+} ion—in its $[Xe]4f^1$ ground state—plus an associated charge-compensating defect, in $LiBaF_3$: (i) Ce^{3+} at a Ba site plus a vacancy at a nearest Li site, (ii) Ce^{3+} at a Li site plus a vacancy at a nearest Ba site, and (iii) Ce^{3+} at a Ba site plus a Li at a nearest Ba site.

The essential improvement we made on the work of Andriessen *et al.*[8] on these configurations is found in the fact that we performed *ab initio* calculations to determine the equilibrium geometry of each of these luminescence centers by optimizing the geometry of a $3\times3\times3$ supercell of $LiBaF_3$ containing a single defect complex.

From each resulting equilibrium geometry a cluster of atoms was taken to calculate the energy of the Ce^{3+} $4f \rightarrow 5d$ absorption lines in these three luminescence center configurations. As can be seen from Tables III, V, and X, only the predicted Ce^{3+} $4f \rightarrow 5d$ absorption lines for the luminescence center configuration consisting of Ce^{3+} at a Ba site, charge compensated by a Li^+ at a nearest Ba site, agree with experiment, albeit not perfectly (4.89, 5.24, 5.49, and 5.87 eV from calculation, versus 4.96, 5.17, 5.69, and 6.08 eV from experiment[6]).

The hypothesis that the relaxation of the lattice around the Ce site in the luminescence center configuration, consisting of Ce^{3+} at a Ba site plus a vacancy at a nearest Li site, would affect the Ce $5d$ crystal-field states to the extent that the ordering of the e and t_2 levels is reversed (see Sec. I), is clearly invalidated (see Table III).

The lattice relaxation around the Ce site in the luminescence center configuration, consisting of Ce^{3+} at a Li site plus a vacancy at a nearest Ba site, was indeed found to be extensive but does not alter the fact that the predicted overall splitting of the Ce $5d$ manifold is much too large compared to experiment (see Table V).

The stability of the cluster Q'_{01a} [see Fig. 6(a) and Table VIII], representing the luminescence center configuration consisting of Ce^{3+} at a Ba site, charge compensated by a Li^+ at a nearest Ba site, was checked with respect to displacements of the Ce ion and its 12 nearest-neighboring F ions, and was found to be satisfactory (no displacements larger than 0.01 Å). This means that both the cluster as well as supercell calculations more or less agree on the same equilibrium geometry for this luminescence center configuration, which is quite encouraging considering the fact that these methods employ completely different ways to model the defect, different Hamiltonians, and different basis sets.

Table VI shows that for this luminescence center configuration the same degree of agreement is found between the

TABLE IX. Q'_{02}, the $CeF_{12}Li_9Ba_{17}$ cluster, representing the luminescence center consisting of Ce^{3+} (in its excited-state configuration) on a Ba site, charge compensated by a Li at one of the nearest Ba sites (all coordinates are in Å).

Ion	x	y	z
Ce	0.00000	0.00000	0.00000
Li	−1.99320	2.00038	1.46080
Li	−1.99320	−1.99320	1.46200
Li	1.99799	−1.99201	1.46080
Li	1.99918	2.00158	1.46200
Li	−1.94535	−1.94295	−2.60815
Li	−1.94654	1.94774	−2.60456
Li	1.94654	−1.94176	−2.60696
Li	1.94774	1.94894	−2.60337
Li	0.00359	0.00718	4.55230
F	−0.00120	−2.00140	1.32681
F	−2.00140	−0.00239	1.32681
F	0.00000	1.99554	1.33040
F	1.99594	−0.00239	1.32920
F	−1.79420	−1.79420	−0.61375
F	1.79420	−1.79420	−0.61256
F	1.79420	1.79420	−0.60299
F	−1.79420	1.79420	−0.61016
F	−0.00239	2.08293	−2.65481
F	−2.09250	−0.00239	−2.65840
F	2.08533	−0.00239	−2.65481
F	−0.00239	−2.09250	−2.66079
Ba	0.00600	3.91940	3.37020
Ba	3.91700	0.01080	3.37020
Ba	0.00720	−3.91700	3.37020
Ba	−3.91700	0.00960	3.37020
Ba	0.00359	3.99478	−0.64845
Ba	3.99358	0.00718	−0.64845
Ba	3.99957	4.00315	−0.62332
Ba	0.00359	−3.99478	−0.65084
Ba	3.99957	−3.98880	−0.62213
Ba	−3.99478	0.00598	−0.64965
Ba	−3.99478	4.00196	−0.62213
Ba	−3.99478	−3.99119	−0.62093
Ba	0.00000	0.00240	−4.40870
Ba	0.00240	3.97920	−4.62400
Ba	3.97680	0.00960	−4.62520
Ba	0.00600	−3.97680	−4.62760
Ba	−3.97920	0.00840	−4.62760

TABLE XI. The Ce^{3+} $5d_{z^2} \rightarrow 4f$ emission line. All results were found from calculations on a cluster with geometry Q'_{02}.

State	Energy (eV)		$5d \rightarrow 4f$ (eV)	
	HF	Orbital	Predicted	Observed
$^2F_{5/2}$	−70859.50896			
$5d_{z^2}$	−70854.43165	−1.84987	4.27921	3.875
$5d_{xz}$		−0.46947	5.65961	
$5d_{yz}$		−0.46893	5.66015	
$5d_{xy}$		−0.31525	5.81383	
$5d_{x^2-y^2}$		−0.14661	5.98247	

splitting of the Ce^{3+} $5d$ manifold as calculated using the supercell method (see Sec. V) and as found from cluster calculations. Also the ordering by character of the Ce $5d$ derived crystal-field states is the same in both the cluster as well as in the supercell calculations.

These observations confirm the conclusion of the previous study by Andriessen *et al.* that the configuration of the luminescence center in $LiBaF_3:Ce^{3+}$, most likely consists of Ce^{3+} at a Ba site, charge compensated by a Li^+ ion at a nearest Ba site.

B. The origin of the unusually large Stokes shift in $LiBaF_3:Ce^{3+}$

For the luminescence center configuration, consisting of Ce^{3+} at a Ba site plus a Li at a nearest Ba site, the relaxation induced by a Ce^{3+} $4f \rightarrow 5d$ excitation was calculated, and from the resulting equilibrium geometry the cluster Q'_{02} was taken (see Fig. 8 and Table IX).

This cluster also was found to be stable with respect to displacements of the Ce ion and its 12 nearest-neighboring F ions (largest displacements ≈ 0.03 Å). This is somewhat surprising in light of the huge displacement shown by the Ce ion in the $Q_{01a} \rightarrow Q_{02}$ relaxation, and considering the fact that Ce has moved to within 2.36 Å of it F neighbors in the $z \approx a_0$ plane (see Fig. 8), which is quite close in comparison with, for instance, the nominal Ce-F distance of 2.68 Å in $BaF_2:Ce^{3+}$.

This agreement in addition to the earlier mentioned results obtained for the splitting of the Ce^{3+} $5d$ manifold (see Table VI) shows that the use of the Ce* pseudopotential to describe Ce^{3+} in its $5d$ configuration is indeed justified.

The energy of the emission from the lowest Ce^{3+} $5d$ crystal-field state to its $^2F_{5/2}$ ground state was calculated to be 4.28 eV [ΔSCF energy between the Hartree-Fock (HF) entries in Table XI], compared to 3.88 eV found from experiment.

The positions of the other Ce^{3+} $5d$ crystal-field states with respect to the emitting state were calculated from the differences in their respective Ce^{4+} virtual orbital energies, as described in Sec. II.

From the cluster calculations on geometries Q'_{01a} and Q'_{02}, and the supercell calculations on Q_{01a} and Q_{02}, we found Stokes shifts of, respectively, 0.607 27 and 0.472 85 eV. The substantial discrepancy between these calculations and the Stokes shift of 1 eV, as found from experiment, will be the subject of discussion in the following section.

The origin of the Stokes shift in $LiBaF_3:Ce^{3+}$ can be explained from examination of the results listed in Tables X and XI, as follows. In geometry Q_{01a} the Ce ($[Xe]4f^1$) ion is more or less twelve coordinated by F^- ions as it would have been in the unrelaxed inverse perovskite structure of Fig. 5. This geometry gives rise to a relatively small crystal field at the Ce site, and consequently to the modest overall splitting of its $5d$ manifold, of 1.12 eV (see Table X). However, in this geometry the derivative of the crystal field at the Ce site, with respect to the displacements shown in the relaxation from $Q_{01a} \rightarrow Q_{02}$, by the Ce ion and its F nearest neighbors in the $z \approx \frac{1}{2}a_0$ plane, is quite large. Any $4f \rightarrow 5d$ excitation of Ce^{3+} will rapidly undergo a nonradiative transition to the lowest Ce^{3+} crystal-field state ($5d_{z^2}$). The before-mentioned displacements ($Q_{01a} \rightarrow Q_{02}$), which cause an increase of the crystal field at the Ce site, almost double the overall crystal-field splitting of the Ce^{3+} $5d$ manifold, from 1.12 eV in geometry Q_{01a} to 1.70 eV in Q_{02} (see Table XI). The $5d$ centroid position shifts only minimally (by 0.04 eV). The ΔSCF energy between the $5d_{z^2}$ crystal-field state and the $5d$ centroid, however, increases by 0.57 eV. These latter two observations show that when the $5d_{z^2}$ state is occupied, the increase in crystal-field splitting of the $5d$ manifold results directly in a lowering of the total energy of the system, thus providing the driving force behind the $Q_{01a} \rightarrow Q_{02}$ relaxation.

VIII. DISCUSSION

In the following we will discuss several aspects of the calculations on the luminescence center configuration, consisting of Ce^{3+} on a Ba site plus a Li^+ on a nearest Ba site (see Sec. VI D), pertaining to the discrepancy between the Stokes shifts of 0.61 eV and 0.47 eV, as found from, respectively, cluster and supercell calculations, and the Stokes shift of 1 eV found from experiment.

A. Cluster calculations

Considering the fact that the cluster calculations on geometry Q'_{01a} yield Ce^{3+} $4f \rightarrow 5d$ optical-absorption energies in close agreement with experiment, the substantial discrepancy (≈ 0.4 eV) between experiment and the predicted $5d_{z^2} \rightarrow 4f$ luminescence energy of Ce^{3+} in geometry Q'_{02}—and hence the same error in the calculated Stokes shift—is quite disappointing. We offer the following tentative explanations.

(i) The basis set that was used in our cluster calculations—and those of Ref. 8 as well—did not contain any polarization functions. Therefore, the polarizability of the ions in the cluster is much too small. In addition to this, the polarizability of the medium surrounding the cluster is not accounted for by our method of point-charge embedding. Therefore, any change in polarization of the cluster or its surroundings, as a result of the $Q_{01a} \rightarrow Q_{02}$ relaxation, is not taken into account in our cluster calculations.

This change in polarization energy was roughly estimated using the GULP (Ref. 25) pair-potential code. To describe the Ba-F, Li-F, and F-F interactions, we used the interionic potentials for $LiBaF_3$ published by Jackson *et al.*[26] The interionic potential describing the Ce-F interaction was largely the same as the one describing the Ba-F interaction, but it was

slightly modified to reproduce the relaxation of the Ce^{3+} ($[Xe]4f^1$) ion in the $+z$ direction, as found in our supercell equilibrium geometry Q_{01a}. To calculate the lattice relaxation induced by the excitation of Ce^{3+}, we simply placed the Ce^{3+} ion at the position it occupies in supercell geometry Q_{02} and kept it fixed, while the rest of the lattice was allowed to relax. The above more or less reproduces the $Q_{01a} \rightarrow Q_{02}$ relaxation we found in our supercell calculations. The change in polarization energy we find as a result of this relaxation is ≈ 0.4 eV. Because of the rough way in which we forced this system to relax, we can take this only to show that the change in polarization energy is of the same order of magnitude as the discrepancy we find between our calculated Stokes shift and experiment.

(ii) Largely due to the insufficient polarizability of the immediate surroundings of the Ce^{3+} ion, i.e., the atoms in the cluster, we do not obtain true Franck-Condon transition energies in our calculations of the Ce^{3+} optical absorption and luminescence energies. (A possible change in the polarization energy, at fixed cluster geometry, due to a Ce^{3+} $4f \rightarrow 5d$ transition—or vice versa—contributes to the energy of the Franck-Condon transition, but is not taken into account in our calculations.)

(iii) When comparing the disagreement of 0.4 eV, between experiment and the calculated $5d_{z^2} \rightarrow 4f$ luminescence energy, with the very reasonable agreement between the calculations on the optical-absorption energies and experiment, one should keep the following in mind. As was explained at the end of Sec. II, our cluster calculations fail to reproduce the centroid shift of ≈ 1 eV commonly observed in fluorides, but this is compensated by the fact that we neglect to take correlation into account. This centroid shift, however, is found from the Ce^{3+} $4f \rightarrow 5d$ transitions observed in optical-absorption measurements. Since we only observe Ce^{3+} $5d \rightarrow 4f$ luminescence from the lowest $5d$ state, and since we are not aware of any excited-state absorption measurements concerning the Ce^{3+} $5d$ manifold, we do not know whether the centroid shift is sensitive to the lattice relaxation induced by the excitation of Ce^{3+}. (The fact that the centroid shift is more or less constant for Ce^{3+} in a range of different fluoride compounds seems to suggest that it is not.) A change in the centroid shift due to lattice relaxation would to some extend invalidate the previously mentioned compensation by the correlation energy, where the calculations of the Ce^{3+} luminescence energy are concerned. Our cluster calculations show a difference of only 0.04 eV, between the centroid shift for Ce^{3+} in cluster geometry Q'_{01a} and Q'_{02}, but this tells us nothing since we fail to reproduce the 1 eV centroid shift between Ce^{3+} in cluster geometry Q'_{01a} and the free Ce^{3+} ion. This, therefore, remains a weak point in these calculations, and one which might contribute to the fact that we cannot predict the Ce^{3+} luminescence energy to the same degree of agreement with experiment as we can absorption energies.

B. Supercell calculations

The Stokes shift found directly from supercell calculations amounts to 0.472 85 eV, which is in disagreement with experiment and differs from the Stokes shift found from cluster calculations. Several factors can play a role here.

(i) Our supercell calculation of the lattice relaxation induced by the Ce^{3+} $4f \rightarrow 5d$ excitation cannot optimize the structure beyond the next-nearest neighbors of the Ce ion. This limit is imposed by the size of the $LiBaF_3$ supercell ($3 \times 3 \times 3$ unit cells). Calculations on, for instance, a $4 \times 4 \times 4$ supercell would include the relaxation of the third and fourth shell of atoms around the Ce ion. Additional relaxation of the lattice beyond the next-nearest-neighbor distance of the Ce ion could very well increase the Stokes shift as calculated directly from supercell calculations. In addition to this, additional relaxation could also affect the immediate surroundings of the Ce ion and consequently the cluster calculation on the $5d_{z^2} \rightarrow 4f$ emission line. Conceivably this would lead to closer agreement between results obtained from supercell and cluster calculations with each other and with experiment.

(ii) The spatially extended defect structure we are considering introduces a large net dipole moment within the supercell. The field of this dipole cannot correctly establish itself when the size of the supercell is insufficient to contain it completely. This is caused by the periodic boundary conditions, which do not allow for a gradual change of the electrostatic potential over distances greater than the size of the supercell. To get an order of magnitude estimation of the consequences of applying the periodic boundary conditions, let us consider an elementary dipole oriented in the $-z$ direction, in the middle of a cubic box of volume L^3. If we take the position of our dipole to be given by the coordinates (0,0,0), then the points $(x,y,L/2)$ $(x,y,-L/2)$ in the top and bottom plane of the box will, respectively, be at electrostatic potential $-V(x,y)$ and $V(x,y)$ (with $V>0$). However, when one applies periodic boundary conditions to this box, there can no longer be a potential difference between corresponding points in the top and bottom plane. This can be seen as if there were an additional electric field in the box—an artifact of the periodic boundary conditions—given by $E = 2V(x,y)/L$, oriented in the $-z$ direction. If we take the moment of the elementary dipole to be equal to the dipole moment of a$+1$ and a-1 charge separated from each other by a distance equal to the distance between the Ce^{3+} dopant ion and the charge-compensating Li in geometry Q_{01a}, and L to be equal to the lattice constant of our $3 \times 3 \times 3$ $LiBaF_3$ supercell, then the artificial electric field at the Ce position in supercell geometry Q_{01a} will be around 0.3 eV $Å^{-1}$. During the $Q_{01a} \rightarrow Q_{02}$ relaxation, the Ce^{3+} ion moves ≈ 0.38 Å in the $+z$ direction and consequently has to deliver around 0.35 eV of work in the artificial electric field. This amount of work is of the same order of magnitude as the disagreement we encounter, between the Stokes shift found from supercell calculations and from experiment.

Of course this is a very rough estimate, since in reality we would have to consider the work needed to move a spatially extended $3+$ charge distribution in an electric field which is neither uniform in the xy plane nor remains constant in the z direction during the relaxation (the relaxation will change the dipole moment in the supercell). Furthermore, in the calculation of the artificial electric field we did not take any dielectric screening of the dipole into account.

However, we can conclude that the presence of this artificial electric field potentially has a large influence on the

results of our supercell calculations on the equilibrium geometries and the Stokes shift. The artificial electric field can be significantly reduced by increasing the size of the supercell, since its magnitude is proportional to L^{-3}.

(iii) The sampling of the BZ in our supercell calculations was limited to the Γ point only, which introduces an unknown error in the results. To check the convergence of the results with respect to the sampling of the BZ, one would like to repeat the calculations using progressively denser **k**-point meshes, or at the least for $\mathbf{k}=(\frac{1}{4},\frac{1}{4},\frac{1}{4})$ instead of the Γ point.

Since at the moment our computational resources do not allow for the above-mentioned increase in supercell size, nor for a different sampling of the BZ, these arguments remain speculative.

ACKNOWLEDGMENTS

This work was partly sponsored by the Stichting Nationale Computerfaciliteiten (National Computing Facilities Foundation, NCF) for the use of supercomputer facilities—Cray C916 of SARA (Academic Computing Services Amsterdam)—with financial support from the Nederlandse Organisatie voor Wetenschappelijk Onderzoek (Netherlands Organization for Scientific Research, NWO). The authors gratefully acknowledge the HPαC (center for High Performance Applied Computing of the Delft University of Technology), for the allocation of time on its Cray T3E. The authors wish to thank G. Kresse for the generation of the Ce pseudopotentials. M.M. further wishes to thank G. A. de Wijs and R. A. de Groot for valuable discussions and help with the supercell calculations.

[1] S. Lizzo, A. Meijerink, G. J. Dirksen, and G. Blasse, Chem. Phys. Lett. **253**, 108 (1996).

[2] S. L. Baldochi, A. M. E. Santo, E. Martins, M. Duarte, M. M. F. Vieira, N. D. Vieira, Jr., and S. P. Morato, J. Cryst. Growth **166**, 375 (1996).

[3] E. Martins, S. L. Baldochi, S. P. Morato, N. D. Vieira, Jr., A. Luci, M. Casalboni, U. M. Grassano, G. Baldacchini, M. Cremona, R. M. Montereali, E. Krausz, and M. Riley, Radiat. Eff. Defects Solids **135**, 15 (1995).

[4] L. Prado, N. D. Vieira, Jr., S. L. Baldochi, S. P. Morato, J. P. Denis, N. Tercier, and B. Blanzat, J. Phys. Chem. Solids **57**, 413 (1996).

[5] M. A. Dubinskii, K. L. Schepler, V. V. Semashko, R. Yu Abdulsabirov, B. M. Galjaut-dinov, S. L. Korableva, and A. K. Naumov, *OSA Tops Proc. on Adv. Solid-state Lasers*, edited by C. R. Pollock and W. R. Rosenberg (Optical Society of America, Washington, D.C., 1997), Vol. 10, p. 30.

[6] C. M. Combes, P. Dorenbos, C. W. E. van Eijk, J. Y. Gesland, and P. A. Rodnyi, J. Lumin. **72-74**, 753 (1997).

[7] C. E. Messer, J. Solid State Chem. **2**, 144 (1970).

[8] J. Andriessen, H. Merenga, C. M. Combes, P. Dorenbos, and C. W. E. van Eijk, in *Proceedings of the International Conference on Inorganic Scintillators and their Applications, SCINT95, Delft, 1995*, edited by P. Dorenbos and C. W. E. van Eijk (Delft University Press, Delft, 1996), p. 142.

[9] M. J. Frisch, G. W. Trucks, H. B. Schlegel, P. M. W. Gill, B. G. Johnson, M. A. Robb, J. R. Cheeseman, T. Keith, G. A. Petersson, J. A. Montgomery, K. Raghavachari, M. A. Al-Laham, V. G. Zakrzewski, J. V. Ortiz, J. B. Foresman, J. Cioslowski, B. B. Stefanov, A. Nanayakkara, M. Challacombe, C. Y. Peng, P. Y. Ayala, W. Chen, M. W. Wong, J. L. Andres, E. S. Replogle, R. Gomperts, R. L. Martin, D. J. Fox, J. S. Binkley, D. J. Defrees, J. Baker, J. P. Stewart, M. Head-Gordon, C. Gonzalez, and J. A. Pople, GAUSSIAN 94 (REVISION C.3) (Gaussian, Inc., Pittsburgh, PA, 1995).

[10] J. Andriessen, P. Dorenbos, and C. W. E. van Eijk, in *Scintillator and Phosphor Materials*, edited by M. J. Weber, P. Lecoq, R. C. Ruchti, C. Woody, W. M. Yen, and R.-Y. Zhu, Materials Research Society Symposia Proceedings No. 348 (MRS, Pittsburgh, 1994), p. 355.

[11] W. J. Stevens, H. Basch, and M. Kraus, J. Chem. Phys. **81**, 6026 (1984).

[12] T. R. Cundari and W. J. Stevens, J. Chem. Phys. **98**, 5555 (1993).

[13] J. P. Desclaux, Comput. Phys. Commun. **9**, 31 (1975).

[14] C. E. Moore, *Ionization Potentials and Ionization Limits Derived from the Analysis of Optical Spectra*, NSRDS-NBS 34, Office of Standard Reference Data (National Bureau of Standards, Washington D.C., 1970).

[15] A. H. Harker, *Hades II/PC: The Harwell Automatic Defect Evaluation System for Personal Computers* (Harwell Publication Office, Oxfordshire, 1989).

[16] G. Kresse and J. Hafner, Phys. Rev. B **47**, 558 (1993).

[17] G. Kresse and J. Furthmüller, Comput. Mater. Sci. **6**, 15 (1996); Phys. Rev. B **54**, 11 169 (1996).

[18] D. Vanderbilt, Phys. Rev. B **41**, 7892 (1990).

[19] G. Kresse and J. Hafner, J. Phys.: Condens. Matter **6**, 8245 (1994).

[20] J. P. Perdew and A. Zunger, Phys. Rev. B **23**, 5048 (1981).

[21] D. M. Ceperley and B. J. Alder, Phys. Rev. Lett. **45**, 566 (1980).

[22] J. P. Perdew and Y. Wang, Phys. Rev. B **45**, 13 244 (1992).

[23] H. J. Monkhorst and J. D. Pack, Phys. Rev. B **13**, 1588 (1976).

[24] C. Combes, Ph.D. thesis, Delft University of Technology, 1999.

[25] J. D. Gale, J. Chem. Soc., Faraday Trans. **93**, 69 (1997).

[26] R. A. Jackson, M. E. G. Valerio, and J. F. Lima, J. Phys.: Condens. Matter **8**, 10 931 (1996).